

Joint Experiments on Small Tokamaks

G. Van Oost 1), M. Berta 2), J. Brotankova 3), R. Dejarnac 3), E. Del Bosco 4), E. Dufkova 3), I. Duran 3), M. P. Gryaznevich 5), M. Hron 3), A. Malaquias 6), G. Mank 6), P. Peleman 1), J. Sentkerestiova 3), J. Stöckel 3), V. Weinzettl 3), S. Zoletnik 2), T. Balázs 2), J. Ferreira 4), A. Fonseca 7), H. Hegazy 8), Y. Kuznetsov 7), A. Ossyannikov 9), A. Sing 10), M. Sokholov 11), A. Talebitaher 12)

- 1) Department of Applied Physics, Ghent University, Ghent, Belgium
 - 2) KFKI-RMKI, Association EURATOM, Budapest, Hungary
 - 3) Institute of Plasma Physics, Association EURATOM/IPP.CR
 - 4) INPE, São José dos Campos, Brazil
 - 5) EURATOM/UKAEA Fusion Association, Culham Science Centre, Abingdon, UK
 - 6) IAEA, NAPC Physics Section, Vienna, Austria
 - 7) Institute of Physics, University of São Paulo, Brazil
 - 8) EAEA, Cairo, Egypt
 - 9) Saint Petersburg State University, Russia
 - 10) Plasma Physics Laboratory, University of Saskatchewan, Canada
 - 11) RRC “Kurchatov Institute”, Moscow, Russia
 - 12) Plasma Physics Research Center, Teheran, Iran
- e-mail contact of main author: g.vanoost@ugent.be

Abstract. The 1st Joint (Host Laboratory) Experiment on “Joint Research Using Small Tokamaks” has been carried out using the IPP Prague experimental facility “CASTOR Tokamak”. The main experimental programme was aimed to characterize the edge plasma in a tokamak by using different advanced diagnostic techniques. It is widely recognized that characterization of phenomena occurring at the plasma edge is essential for understanding of the plasma confinement in a tokamak. The edge plasma in small and large scale experiments has many similar features, and the results obtained through detailed measurements in a small flexible device such as CASTOR are in many aspects still relevant to those in large tokamaks. Therefore, it is expected that results of this joint experiment will have a general validity.

1. Introduction

The first Joint (Host Laboratory) Experiment (JE) on “Joint Research Using Small Tokamaks” (JRUST) involving twenty scientists from seven countries has been carried out between 28 August and 9 September 2005 on the CASTOR at the Institute of Plasma Physics of the Academy of Sciences of the Czech Republic (IPP-ASCR), and was jointly organized by the IPP-ASCR and KFKI (Central Research Institute for Physics of the Hungarian Academy of Sciences) Budapest. It was coordinated by the International Atomic Energy Agency (IAEA) in the framework of the Coordinated Research Project JRUST and supported through the IAEA and the ICTP (International Centre for Theoretical Physics). The objective of the joint experiment was to perform studies on the topics of plasma edge turbulence and plasma confinement based on broad international participation to benefit from the added value of international expertise exchange. The edge plasma studies have a long tradition on the CASTOR tokamak (appropriate equipment, recognized expertise, etc) [see e.g. 1, 2]. Another goal of this joint experiment was the development of tools for remote participation and data exchange. These two aims are expected to follow and contribute to some extent to a pool of knowledge in support of the ITER project, as the JE has been performed under an intensive international cooperation and with an important component of remote operation and data exchange. The role and contribution of small tokamaks to the topics of expertise exchange and remote operation is highlighted by this initiative.

2. Experimental set-up

The particular feature of the experiment is the exploitation of unique diagnostics to study the physics of the edge plasma in detail. During the experiments, electric fields were generated by biasing an electrode inserted into the edge plasma to modify the turbulence and transport behavior in this region. The CASTOR tokamak ($R= 0.4$ m, $a= 0.085$ m, $B_t < 1.5$ T, $I_p < 25$ kA, $\Delta T < 50$ ms, $0.5 < n_e(10^{19} \text{ m}^{-3}) < 3.0$, $T_e(0) < 200$ eV) is equipped with a circular cross section poloidal limiter, and with a standard set of diagnostic tools. During these joint experiments the available diagnostic systems were two bolometric arrays for fast measurement of radiation losses, Langmuir probe arrays for edge plasma monitoring in radial and poloidal directions, directional probes (Gundestrup) for parallel and perpendicular plasma flow determination, and a full poloidal array of magnetic pick-up coils and Hall sensors for plasma position monitoring. The H_α diagnostic was located at the top of the vessel at the same toroidal location of the rake probes to monitor the radiation due to recycling with a sampling frequency of 40 kHz. The data acquisition system consists of 24 channels (40 kHz) to measure the basic plasma parameters and 96 channels (1 MHz) for fast measurements of the edge plasma parameters. The software developed for data acquisition control and for data processing is based on widely used IDL and/or MATLAB environment.

3. Experiments and results

3.1. Radial edge turbulence structure

The time evolution of the radial profiles of electron temperature and density were measured during a single shot. From the signals time shift between two poloidally separated tips it was possible to measure the poloidal velocity of fluctuating density and plasma floating potential structures. Since these time shifts were typically lower than the sampling rate (1 μ s), two statistical techniques were developed allowing the determination of the correlation length and phase velocity of potential fluctuations during a single shot: (i) polynomial curve fitting (fitting the cross-correlation by some polynomial function), and (ii) linear fitting of the phase function of the cross-power spectral density). Both techniques provided similar results, as illustrated in Fig.1. Both methods diverge in the proximity of the Last Closed Flux Surface (LCFS), which is associated with the maximum of the floating potential seen in the left panel of figure 1. However, the position of the velocity shear layer (VSL) can be identified with a precision ~ 1 mm, as it is evident from Fig. 1. From the gradient of floating potential (dashed line in the left graph of Fig. 1), the phase velocities were roughly estimated as $v = E_r/B$, where E_r is estimated as $\text{grad } \Phi_f$, neglecting the gradient of the electron temperature. In the right graph of Fig. 1, the velocities are depicted as three horizontal lines (in the region $50 < r < 60$ mm $v_{\text{ph}} = -1.4$ km/s, for $60 < r < 70$ mm $v_{\text{ph}} = -3.3$ km/s, and for $70 < r < 90$ mm $v_{\text{ph}} = 1.3$ km/s). The experimental points are above these lines implying that the electron temperature gradient can not fully be neglected, if a precise comparison of the phase and $E \times B$ velocity is required. The phase velocity of density fluctuations is systematically lower than that of potential fluctuations. From the spatio-temporal behavior of cross-correlation functions of radially separated tips, a radial size of the fluctuating structures of about 1 cm was determined.

3.2. Poloidal edge turbulence structure

The phase velocity of potential fluctuations in the poloidal direction was measured in discharges with and without biasing using a poloidal array of 96 Langmuir probes arranged uniformly poloidally in one toroidal position. Due to a limited number of digitizers only 32

channels could be measured simultaneously. In most measurements every third probe was used, but occasionally the local structure was studied by digitizing all signals from a limited poloidal range. Data measured by the poloidal ring were evaluated by correlation techniques. A typical correlation plot is shown in Figure 2, where the x axis is the time lag and the y axis is the poloidal angle.

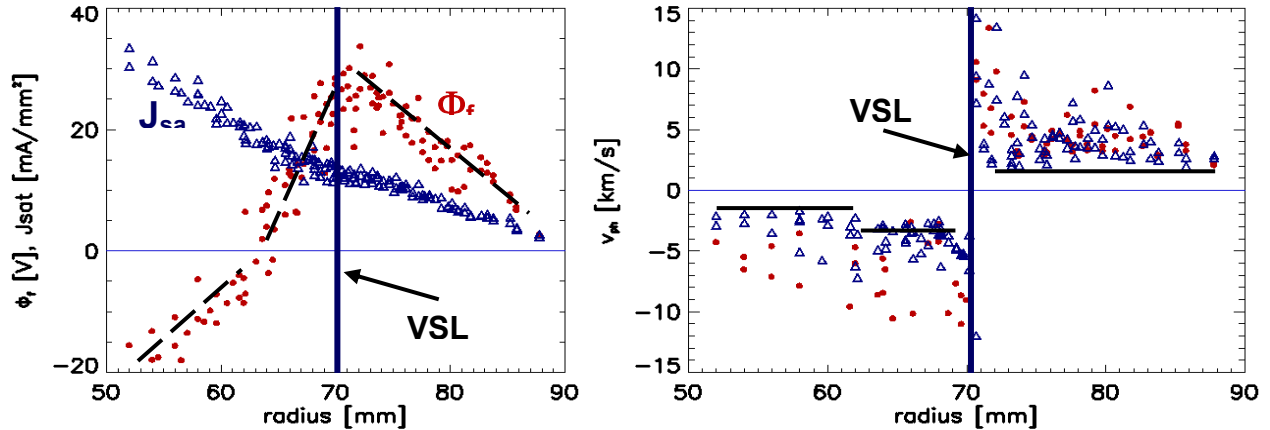


Fig. 1. Left graph: Radial profiles of floating potential Φ_f (red circles), and density of ion saturation current J_{sat} ($J_{sat}=I_{sat}/A$, A is $2 \cdot \pi \cdot \text{radius}$. length of the probe). Right graph: Phase velocities v_{ph} obtained from Φ_f (red circles), and J_{sat} (blue triangles). The horizontal lines in the right graph demonstrate velocities obtained from the simple calculation from the gradient of the Φ_f .

Crosscorrelation between the probes on the poloidal ring
Shot no. 26829 Reference angle: 33./500 Degree

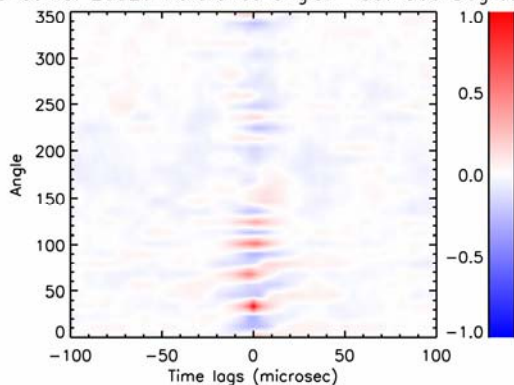


FIG. 2. A spatio-temporal correlation function along the poloidal ring of probes. The reference probe is at 33.75° relative to the equatorial plane on the LCFS.

Spatial wave-like structures (electromagnetic features of certain turbulence) were observed in the correlation figures in the range between 355 and 135° (0° is on the low field side). In other regions (e.g. at the top) the wave-like structure was not obvious but a localized correlation extending over a couple of probes was seen. The difference in behavior at different locations is believed to be due to misalignment of the probe array relative to the LCFS. In order to determine the temporal change of the amplitude of the wave-like structure the spatial correlation functions were used as filter functions. The filtered signal is highly intermittent and pronounced peaks (above than 3σ) can often be seen, in contrast with the signals of the individual Langmuir probes which are very close to Gaussian. This demonstrates that the temporal behavior of the wave-like poloidally extended structures is very much different from that of the local turbulence and that over the whole array the signal in a certain Langmuir probe is composed of a mixture of these two components: one with a short poloidal correlation (cm scale) and another one with wave-like character correlated over. The mode number of this wave-like phenomenon approximately matches the edge safety factor value. A long toroidal correlation length (correlation value above 0.8 over one half of the toroidal circumference) between certain rake probe and ring probe pins could be observed, when these pins were located on the same flux tube.

3.3. Magnetic measurement using array of low-cost commercial Hall sensors

As the discharges became longer in large tokamaks, the evaluation of B from its measured time derivative has become increasingly difficult, because the integration needs a precise determination of possible offsets in the preamplifiers. Recently, *Hall probes* have been used to measure the absolute value of B directly together with its fluctuations in the boundary plasma of tokamaks [4]. Advancements in semiconductor technology hand in hand with a broad spectrum of industrial applications have driven development of new types of Hall sensors for magnetic measurements in recent years. Particular advancement is the availability of ‘integrated’ Hall transducers, where the sensing element together with complex electronic circuitry is integrated on a single small chip with characteristic dimension of a few millimeters. The on-chip integrated circuits provide stabilization of the supply voltage, output voltage amplification, signal conditioning in order to suppress the high frequency noise, and elimination of temperature dependence of the sensor’s output. Particularly, output amplifier placed directly next to the sensing element significantly improves the frequency response and improves signal to noise ratio. The 16 Hall sensors of A1322LUA type produced by Allegro MicroSystems, Inc. were mounted on a stainless steel ring symmetrically encircling the CASTOR plasma in poloidal direction 10 mm outside the limiter radius. The Hall sensors were oriented so that they measure poloidal magnetic field. The special adjustable holders were used in order to ensure proper alignment and consequently to minimize the cross talk from about 50 times stronger toroidal magnetic field. A traditional magnetic pick-up coil was fixed nearby each Hall sensor for reference and also for envisaged MHD studies. The sensors have a nominal sensitivity of 31.25 mV/mT and dynamic range ± 80 mT. The peak-to-peak noise level is below 1mT. The bandwidth specified by manufacturer is 30 kHz. The operating temperature range is from -40°C to 150°C . A supply voltage of 5V is needed to drive each Hall sensor. The sensor calibration in a frequency band 1-20 kHz is plotted in Fig. 3.

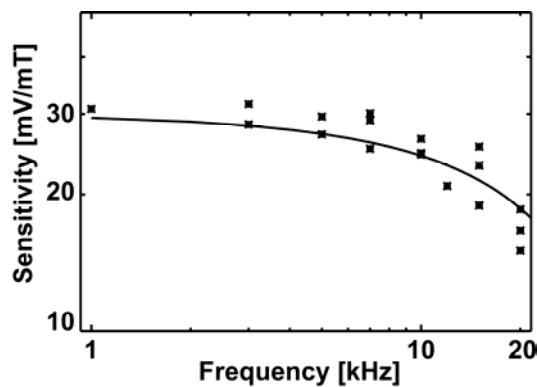


FIG. 3. Calibration curve of the A1322LUA Hall sensor in the frequency band 0-20 kHz.

The frequency response of the sensors was found to be reasonably flat up to 10 kHz, which is sufficient e.g. for plasma position measurements on CASTOR. Additionally, DC calibration of each Hall sensor was performed using standard Helmholtz coils. The importance of the planar Hall voltage generated by a strong toroidal magnetic field (~ 1.2 T on CASTOR) oriented parallel to the sensor’s plane was investigated. For this purpose were performed several vacuum field pulses charging only poloidal field coils creating a known calibrating magnetic field. In addition, the toroidal field coils were energized, creating a toroidal magnetic field perpendicular to the calibration magnetic field. The difference in the sensor’s output with and without the toroidal magnetic field was well below the noise level. Therefore, the contribution of the planar Hall effect to the sensor’s output voltage was found to be negligible. On CASTOR the sensors are operated at rather stable temperature close to the room temperature. Nevertheless, the possible temperature dependence of the sensor’s output was checked having in mind the possible use of these sensors in middle-sized fusion devices, where temperature variations over a single pulse can become significant. In conclusion, the A1322LUA type integrated Hall sensors produced by Allegro MicroSystems, Inc. were tested for the first time in tokamak environment on CASTOR, and they are found to qualify for in-vessel use of small to middle sized fusion

devices where the radiation is not an issue. They offer an attractive alternative to traditional pick-up coils for applications where the good frequency response up to 10 kHz is sufficient and the temperature below 150°C can be guaranteed. The main advantages over the traditional pick-up coils are the smaller size and more straightforward interpretation of output without the need of rather cumbersome integration and drift removal procedure associated with the use of inductive loops. Further exploitation of these sensors on CASTOR is envisaged particularly to improve precision of plasma position measurement.

3.4. Edge biasing

Figure 4 presents results of the effects of the edge electrode positive biasing on the main plasma parameters. The figure shows time traces of the electrode voltage (V_E) and current (I_E), central line-averaged density \bar{n}_e , H_α emission and the ratio of \bar{n}_e/H_α . Before biasing, the electrode (inserted from the top and positioned at radius $r_E=40\text{mm}$) was floating so that no current flowed between the electrode and the vessel. At about 10 ms of the plasma discharge, a positive biasing pulsed voltage $V_E \approx 260\text{ V}$ is applied for a period of $\sim 5\text{ ms}$, during which an average current of about $I_E = 20\text{ A}$ is drawn by the electrode, as seen in Fig. 4(a). In Fig. 4(b), it can be seen that during biasing, \bar{n}_e is built-up gradually and reached $1.7 \times 10^{19}\text{ m}^{-3}$ at $t = 14\text{ ms}$ before slowly falling off to its original pre-bias value. In the initial stage of the biasing, from 10 to 12.5 ms, there is a clear reduction in recycling indicated by a drop in H_α emission, and thus, a net increase of the ratio \bar{n}_e/H_α (which is roughly proportional to the particle confinement time τ_p) by a factor of 2.5 with respect to the pre-bias phase, as can be seen in Fig. 4(c) and (d), respectively. These results indicate an improvement of the global particle confinement induced by the electrode positive biasing, as observed earlier. [3]

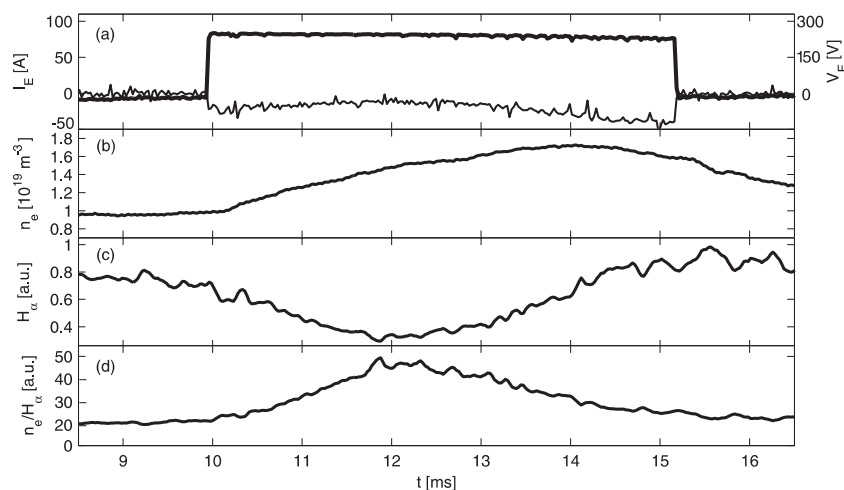


FIG. 4. Time evolution of plasma parameters of a typical edge electrode biasing experiment on CASTOR. (a) the electrode voltage V_E (thick line) and current I_E (thin line), (b) the central line-averaged electron density \bar{n}_e , (c) H_α radiation, and (d) the ratio of \bar{n}_e/H_α .

Figure 5 further illustrates the influence of the positive biasing on the radial dependence of edge plasma parameters. The radial profiles of the floating potential ϕ_f , radial electric field E_r and its shear dE_r/dr , and ion saturation current I_s are obtained by averaging over a time window of 4 ms before (open symbols) and during (filled symbols) the biasing phase. Here, E_r is calculated directly from the radial derivative of ϕ_f measured at $r=60\text{mm}$ on two adjacent pins neglecting the contribution from the T_e gradient, and therefore underestimating E_r slightly. The radial position of the LCFS is around $r_{\text{LCFS}} = 66\text{ mm}$ (indicated by dash-dotted line in the figures). During the biasing phase, the radial dependence of ϕ_f is strongly

modified as shown in Fig. 5(a), leading to a narrow positive and single-peaked E_r structure with a maximum of 11 kV/m at $r \approx 61$ mm, just inside the LCFS (see Fig. 5(b)). As a consequence, a strong positive ($\sim 1.3 \text{ MV/m}^2$) and negative ($\sim -1 \text{ MV/m}^2$) E_r shear is generated inside and across the LCFS, respectively, as shown in Fig. 5(c). The maximum shear rate of the $E_r \times B$ flow, $\tau_s^{-1} \propto dv_{E_r \times B}/dr$, is thus about $1\text{-}1.3 \times 10^6 \text{ s}^{-1}$. On the other hand, the decorrelation rate of local turbulence scattering, τ_{c0}^{-1} , calculated from the e-folding time of the autocorrelation function of I_s fluctuation data detected before biasing, gives $\tau_{c0}^{-1} = 1.6 \times 10^5 \text{ s}^{-1}$. Hence, the flow shear rate exceeds significantly the turbulence scattering rate and thus suppresses turbulence and turbulent transport. The reduction in I_s and ϕ_f fluctuations during biasing has been observed in the experiments. The reduced turbulent transport leads to the formation of an edge pedestal and thus steepening of the edge density profile during biasing, as shown in Fig. 5(d). It can be concluded that a clear and reproducible transition to an improved confinement is induced by the edge electrode biasing along with a creation of a particle edge transport barrier just inside the LCFS. This barrier is characterised by a (i) substantial increase of the edge density gradient; (ii) reduction in recycling indicated by a drop in H_α signal; (iii) substantial increase of the global particle confinement time; (iv) suppression of the density and potential fluctuation level.

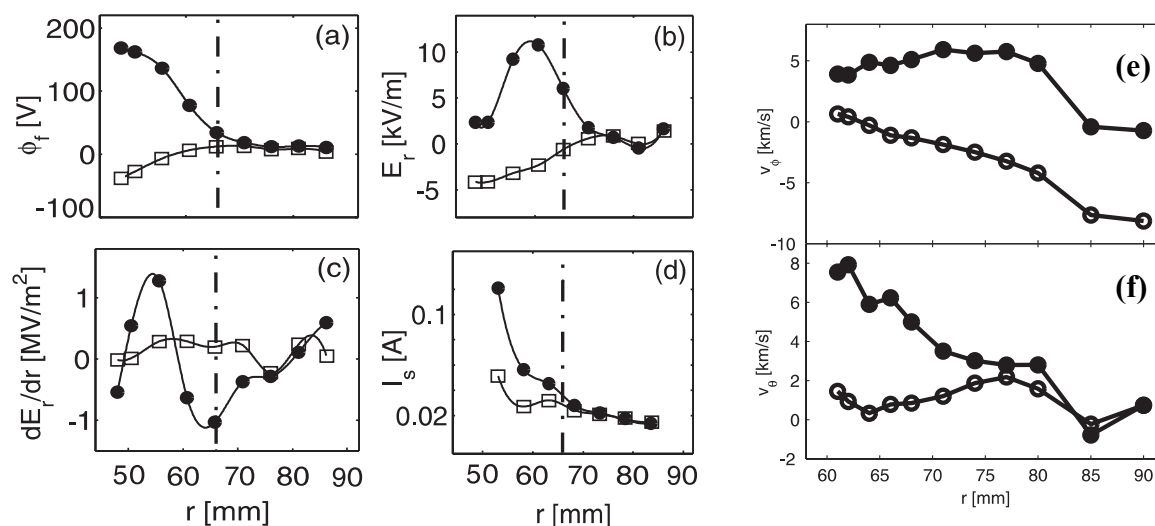
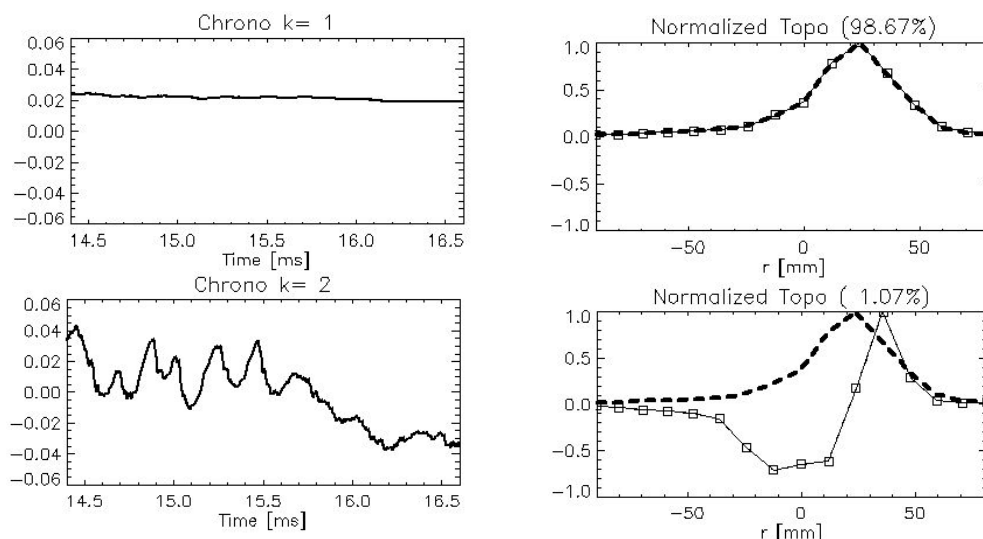


FIG. 5. Radial profiles of the (a) floating potential ϕ_f , (b) radial electric field E_r , (c) E_r shear, and (d) ion saturation current I_s (e) toroidal velocity v_ϕ and (f) poloidal velocity v_θ averaged over 4 ms before (open symbols) and during (filled symbols) biasing. The vertical dash-dotted line marks the position of the LCFS.

Flow measurements were performed using a Gundestrup probe with 8 collectors [5]: the time evolution of the radial profiles of floating potential, radial electric field, parallel and perpendicular Mach numbers were measured in the biased and ohmic phases of a single discharge. The radial flow profiles were measured by a shot-to-shot scan in reproducible discharges. It is found that not only the perpendicular flow, but also the parallel flow increases during biasing as shown in Fig.5(e) and (f).

3.5. Radiation fluctuations and profile measurements with fast bolometry

Two arrays of fast AXUV-based bolometers with 16 and 19 channels were installed in the same poloidal cross-section in mutually perpendicular directions (from LFS and bottom side) to monitor the radiated power profile. This arrangement with unique temporal resolution of 1 μs and spatial resolution of about 1 cm and a very high signal to noise ratio allowed a visualization of fine structures on the radiated power profile. First, the measured AXUV data are typically used to find the evolution of the total radiation, radiation peak position (shift), radiation FWHM and the brightness profile [6]. Afterwards, the data are separated into spatio-temporal components by the Singular Value Decomposition method (SVD) [7]. In this way, components with a different spatial or temporal behaviour can be distinguished from each other and they were here interpreted as the dominating main plasma profile ($k=1$), a poloidally rotating asymmetric component ($k=2$) and radial structures corresponding to symmetric component ($k=3$), see Fig. 6. A high contrast between the $k=1$ component and higher ones, usually of the order of the weight ratios 99.6:0.3:0.05, is observed for a typical ohmically heated CASTOR plasma. With biasing, higher components are amplified up to 98.5:1.1:0.2, as shown at the end of the biasing phase in Fig. 6. Topos, spatial eigenvectors, show a type of the evolution (amplitude change, poloidal or radial movement) and a localization of each structure, meanwhile chronos, temporal parts, indicate their presence, amplitude and periodicity. In Fig. 6, a vanishing of the 6 kHz radial and poloidal structures is observed after the end of the biasing phase. The method based on SVD applied on fast bolometric data, developed during the present experiment, was later used for the analysis of snake-like structures after pellet injection in the T-10 tokamak [8]. Another method to process fast bolometric data is the analysis of the fluctuating part of raw data obtained by subtracting the mean value. The data are chord integrated, thus the result does not correspond to the evolution of single local turbulent event but to their sum along the whole chord. By the auto-correlation analysis, the event frequency can be obtained from the periodicity of the auto-correlation function. The cross-correlation of one channel with neighboring ones in principle gives the velocity and the movement direction, while the cross-correlation with a perpendicular bolometric chord gives the localization of the event. As an illustration, the cross-correlation analysis (horizontal chord at 40 mm against bottom chords) of shot #26991 with a biasing period at 10-15 ms is shown in Fig. 7. Prior to biasing, clear structures with repetition frequency about 30 kHz are present. During biasing, the periodicity is destroyed, but the surface near radius 50 mm shows a high level of correlation indicating the presence of a well-localized structure. A few milliseconds after the end of biasing, the periodicity is still not restored, however a well-correlated, radially moving event is registered.



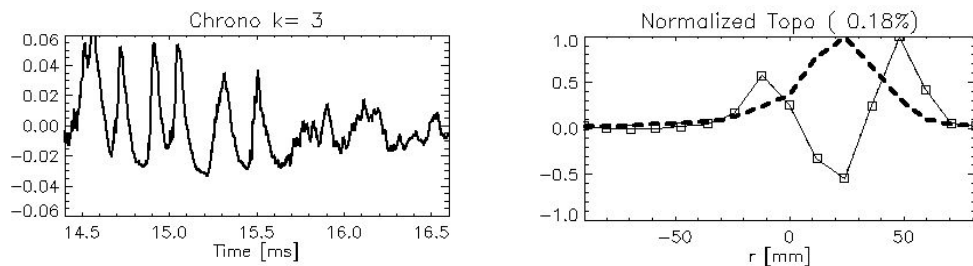


FIG. 6. Example of fluctuations analysis of fast bolometric signals from the bottom AXUV array with $1\mu\text{s}$ temporal and 1 cm spatial resolution in a shot with edge plasma biasing (#26995, $r_E=60\text{mm}$, $U_B=+250\text{V}$). Temporal and spatial eigenvectors of the first three significant components of the SVD are compared with an averaged emission profile (dashed line). Chronos (on the left) show temporal behaviour of the radiation losses which can be divided into a dominating quasi-stationary spatial part ($k=1$), a rotating asymmetric component ($k=2$) and radial structures ($k=3$). Normalized energies(weights) of each component are given in brackets. Open squares on topos represent chord radii of the individual bolometric channels.

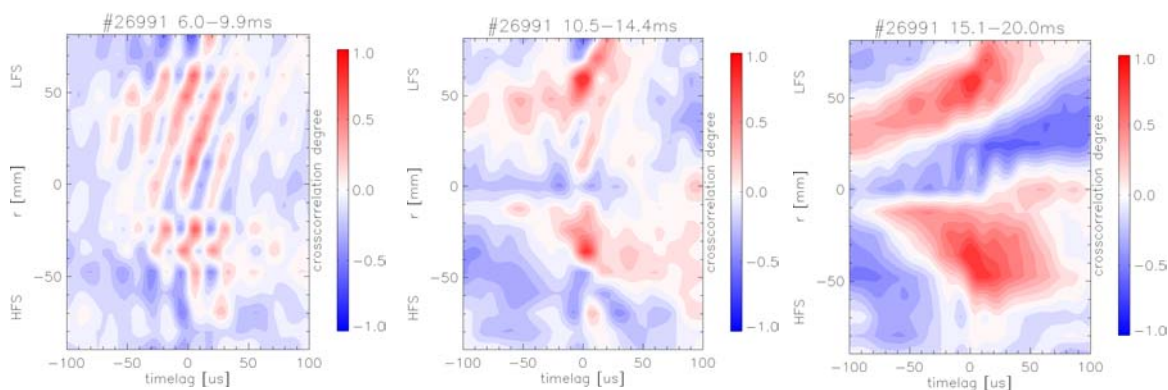


FIG. 7. Cross-correlation between one horizontal chord at 40 mm against all bottom chords show moving structures in the shot #26991. Prior to biasing (left graph), the presence of the periodic events with frequency 30kHz and velocity 2.3 km/s are demonstrated. During biasing with biasing voltage $+150\text{V}$ (middle graph), the surface near radius 50 mm shows a high level of correlation indicating the presence of well-localized structure. After biasing (right graph), a well-correlated, radially moving event is registered.

References

- [1] DEVYNCK P. et al., Plasma Phys. Control. Fusion 47 (2005) 269.
- [2] STOCKEL J. et al., Plasma Phys. Control. Fusion 47 (2005) 635.
- [3] VAN OOST G. et al, Plasma Phys. Contr. Fusion, 45 (2003) 621, and references therein.
- [4] DURAN I., Stockel J., Mank G., Finken K.H., Fuchs G., Van Oost G., Review of Scientific Instruments, 73, 2002, No. 10, 3482.
- [5] PELEMAN P. et al., International Conference on Plasma Surface Interactions (PSI), Hefei Anhui, China (2006), to be published in J. Nucl. Mat., and references therein.
- [6] DUFKOVA E. et al, 32nd EPS Conference on Plasma Phys. Tarragona, 27 June - 1 July 2005, ECA Vol.29C, P-2.074 (2005).
- [7] DUDOK T. et al, Phys. plasmas, Vol.1, No.10, October 1994, 3288-3300.
- [8] WEINZETLL V. et al, 33nd EPS Conference on Plasma Phys. Rome, 19-23 June 2006, ECA, P-4.080 (2006), in print.